



## **The Influence of No-Core Fiber Length on the Sensitivity in Fiber Optic Strain Sensor**

**Mohammad M. Hasan<sup>1,\*</sup> and Hanan J. Taher<sup>1</sup>**

*\*Corresponding Author: [Mohammad.muzahim@gmail.com](mailto:Mohammad.muzahim@gmail.com)*

*1- Institute of Laser for Postgraduate Studies, University of Baghdad, Baghdad, Iraq.*

(Received 16/6/2021; accepted 10/8/2021)

**Abstract:** The influence of sensing element length of no-core fiber strain sensor has been studied and experimentally demonstrated, four different lengths of 125  $\mu\text{m}$  diameter no-core fiber is fused between two standard single-mode fibers and bi-directionally strained, the highest obtained sensitivity was around  $16.37 \text{ pm } \mu\text{e}^{-1}$  which was exhibited in the shortest no-core fiber segment, to the best of our knowledge this is the first study of the influence of no-core fiber strain sensors length on sensor sensitivity. The proposed sensor can be used in many opto-mechanical applications such as, structural health monitoring, aerospace vehicles and airplane components monitoring.

**Keywords:** optical sensor, strain, and Mach-Zehnder

### **1. Introduction:**

In the past two decades a large number of fiber-optic sensing devices were investigated and developed. These developed sensors are used to sense a various measured such as, refractive index [1], Hydrogen [2], temperature [3], relative humidity [4], biological parameters [5], displacement [6]. Fiber-optic sensors for mechanical application have been rapidly developing and taking a great share in the current research trends, because of the current advancement in modern technology, precision and superiority in sensing system became a must, this led to developing many opto-mechanical fiber sensors such as, fiber bend sensors [7], fiber load sensor [8] fiber torque sensor [9], and fiber strain sensors [10]. The operation technique of opto-mechanical sensors is reliant on the change of the

refractive index of the fiber-optic sensor due to the effect of various mechanical forces, this phenomenon is called the photoelastic effect, the changes in the dimensions of the sensing fiber will change the refractive indices as a result, the shape of the emerging spectrum will change accordingly, The advantages of fiber Opto-mechanical sensors includes, compactness that makes it easier to embed in several systems [11], the immunity to the electromagnetic interference which makes the sensor superior to electronic sensors [12], the inertness to the vast majority of chemicals which is an ideal property of operation especially in engines and gas turbines, the lightweight of fiber sensors which is advantageous as compared to bulky sensors, and the precision which is a vital property in fiber sensors [13]. Multimodal no co-core fibers (NCFs) have been widely investigated in optical fiber sensors, these

fibers come with different diameters and have been showing interesting results in several sensing systems [14, 16]. As these types of fibers have no core, no cladding etching is required to promote more evanescent wave penetration to the surrounding for sensitivity enhancement as compared to typical multimode fiber (MMF). The glass waveguide of NCFs is in a direct contact with the outer media, thus better sensitivity can be achieved [17].

In MMF sensors, the most influential parameters in the sensing segment are the length and the diameter, studying one of these variables might be achieved by fixing the other one. In many published previously works, strain sensor length has been imposing a direct influence on the sensitivity and the performance of the sensor accordingly, optimizing the best length for the fiber-optic sensing segment will greatly improve the sensitivity and the linearity of the fiber sensor [18-20].

In this work, four different lengths NCF based strain sensors principled on Mach-Zehnder interferometer were fabricated and experimentally demonstrated, the used NCF has a diameter of 125 $\mu$ m which is fixed in our experiment, the transmission spectrum characteristic is studied for each length and compared to each other. All NCF sensors were tested in the same laboratory condition at 25 °C utilizing same testing condition. The shortest segment of 3.1 cm length exhibited the highest sensitivity of 16.37 pm  $\mu$ e<sup>-1</sup> and a high linear regression coefficient of 0.9997. To the best of our knowledge this is the first study of NCF multimode fiber length influence on the sensitivity, the proposed sensor can be utilized in various opto-mechanical sensing system for being simple to fabricate, easy to repeat and cost effective with no complexity in structure.

## 2. Theory and Principle

The proposed NCF strain sensors represent a simple Mach-Zehnder interferometer based on multimodal interferometer, an illustrative general graph for the structured sensors is depicted in figure (1),

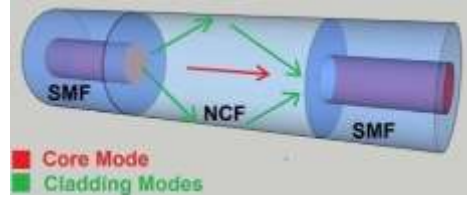


**Figure (1):** Schematic of the NCF strain sensor

and hits the first fusion splicing joint higher order modes is excited, these mode will suffer various reflections on the NCF-air interface and interference phenomenon will occur between different traveling mode due to the phase and speed differences of these modes. These several traveling modes will eventually undergo another recouple when they reach the second fusion splicing joint of the NCF-SMF and emerge to the lead-out SMF [21].

The pattern of the he interference amongst the higher order modes and the fundamental mode can form minima's or maxima's which are dips or peaks. Relying on to the theory of multimodal interference the length of the sensing segment NCFs can be calculated as [22].

$$L = R \left( \frac{3L_b}{4} \right) \text{ with } R = 0,1,2, \quad (1)$$

where,  $R$  is the self-image number and  $L_b$  represents to the length of the corresponding beat

$$L_b \cong \frac{4n_{NCF}D_{NCF}^2}{3\lambda_0} \quad (2)$$

Where,  $n_{NCF}$  represents the refractive index of the no-core fiber and  $D_{NCF}$  is equivalent to the diameter of the no-core fiber, and  $\lambda_0$  is the free space wavelength. Combining the above equations, the free space wavelength can be determined by the below expression.

$$\lambda_0 = R \left( \frac{n_{NCF}D_{NCF}^2}{L} \right), \text{ with } R = 0,1,2, \quad (3)$$

## 3. Fabrication and setup

### 3.1 Sensors Fabrication

A Schematic configuration of the experimental setup is given in figure (2). In pursuance to fabricate the NCFs strain sensors which is simple and non-complex, a piece of 125  $\mu$ m diameter NCF (Thorlabs, FG 125 LA) is fusion spliced amongst dual SMF pigtails, the used SMFs are standard (corning, SMF-28) of 1 meter length.

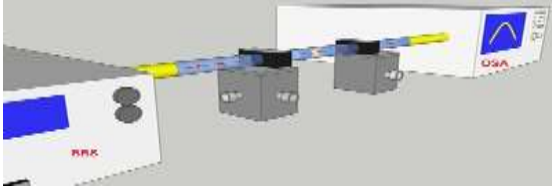


**Figure (2):** Experimental configuration of NCF strain sensors

Best fusion splicing conditions are maintained to get 0 dB loss on both joints by good cleaving and cleaning, the used fusion splicer is (Fujikura, 60S). The setup is mounted on a two (Thorlabs, HFF003) fiber clamps, the fiber clamps then fixed to a grooved wooden foundation by glue, finally the wooden foundation are fixed to a couple (Newport ,XYZ micrometer stages) using screws to ensure excellent system rigidity on three dimensional axes, its necessary to mention that optical alignment in all-axes is vital in fiber strain sensing systems as any bend in the sensing fiber can greatly alter the result and impair the accuracy.

In our work we fixed Z, and Y axes to allow the axial strain to be applied only toward the X-axis. Then, the lead-in SMF is coupled to broadband light (Thorlabs SLD1550S-A1) and the lead-out is connected to an optical spectrum analyzer (Yokogawa, AQ6370). The experiment initiated by inducing axial force in steps of 100  $\mu\text{m}$  to each micrometer toward X-axes in opposite direction by rotating the X-axis lever of each X-Y-Z micrometer stage, doing so makes the total count of one strain step to 200  $\mu\text{m}$ . The Initial distance between the two fiber clamp edges was 40000  $\mu\text{m}$ . The utilized OSA has a resolution of 0.2 nm whereas the spectral range of the used BBS is 1450-1650 nm .The laboratory images of the setup are illustrated in figure (3).



**Figure (3):** Laboratory images of testing setup of all NCF strain sensors

### 3.2 Transmission spectra of NCF sensors

The fabrication process of all NCF strain sensors was similar except of the use of different length. In the examination of the transmission spectra for different sample lengths, no beneficial Mach-Zehnder interferometer could be obtained in the 2 cm range and from 4 cm range and above, in the two cm NCF sensing length the interference dip was small with a low extinction ratio, and in 4 cm length the dips were saw shaped, overlapped and adjacent. Small dips can vanish during experiments while saw shaped dips and adjacent dips can overlap and induce inaccurate results, accordingly our sensing ranges focused mainly on the 3 cm range, the transmission spectrum of various sensing length is given in the figure (4).

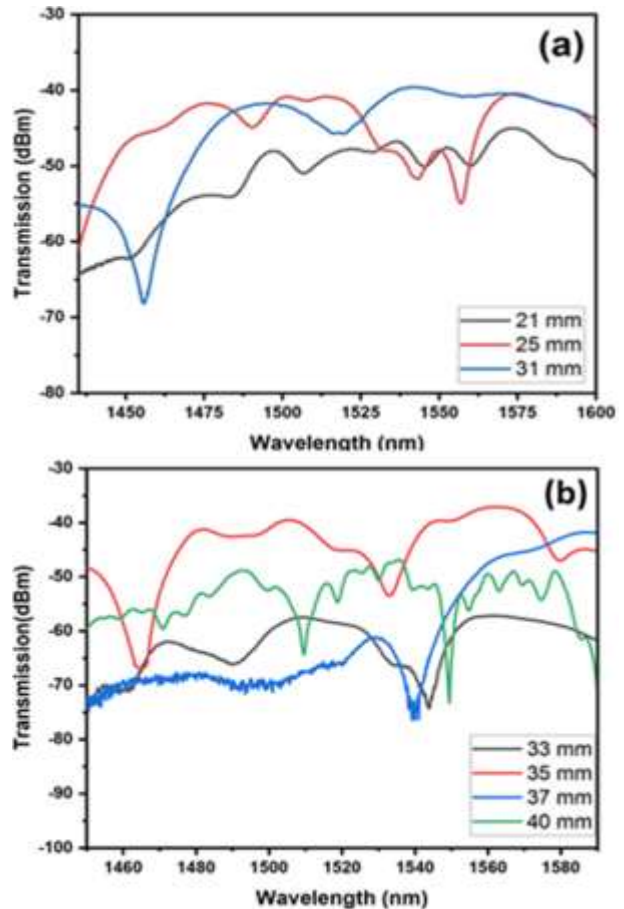


**Figure (4):** Transmission spectra of various NCF sensor lengths ;(a) from 21 - 31 mm and (b) from 33 - 40 mm

From figure (4), 3 cm range sensors (3.1-3.7) revealed good interference dips with good

extinction ratios, the dips are not adjacent or overlapped. Relying on these characteristics each NCF sample sensitivity is examined and the sensitivities are compared to find out the best sensor.

#### 4. Results and discussions

Each NCF sample is examined by situating the sensor on the micrometer stages and clamped by HFF003 fiber holders. Then, the lead-in SMF coupled to the infrared (BBS) and the lead-out is coupled to the optical spectrum analyzer (OSA), axial bi-directional strain applied by rotating each X-axis micrometer stages in steps of 100 μm per each direction, which makes the total count of one steps 200 μm, the spectral shift of the 3.1 cm sensor is illustrated in figure (5). The interference minima exhibited a linear blue-shift with increasing strain from 0 -1000 με in steps of 200 με. The initial distance was 40000 μm between the two fiber clap edges. The examination carried out at room temperature 25 °C. axial strain is determined as [23].

$$\Delta\mu\epsilon = \frac{\Delta L}{L} \times 10^6 \quad (4)$$

where Δμϵ is the applied strain to the NCF sensor, ΔL is the varying length of the sensor, and L is the initial distance between two fiber holders edges.

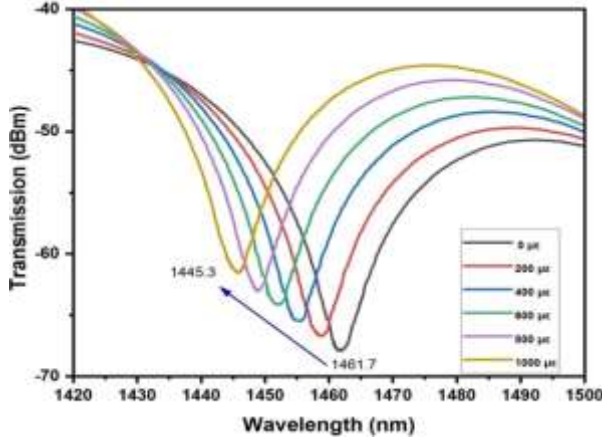


Figure (5): Spectral shift of the 3.1 cm NCF strain sensor.

From the obtained results of the 3.1 cm sample NCF, the linear fitting graph is plotted. This sensor revealed an interference minima at 1461.7, the extinction ratio of the interference dip was around 17 dB, the 3.1 cm NCF strain sensor revealed a very good linearity with strain, the linear regression coefficient R<sup>2</sup> is 0.9997 for

strain. The attained strain sensitivity was as high as -16.27 pm / με. The linear fitting plot of the 3.1 cm sample is depicted in figure (6). The interference minima of the 3.1 NCF sensor exhibited wavelength shift due to the variance of the refractive indices of several propagating modes along the NCF segment, this variance is mostly induced as a response to the photo-elastic effect of the NCF fiber segment. Since tensile force can make the length of the NCF fiber sensor to change slightly. Consequently, the effective refractive indices between the core mode and the higher order modes will suffer a relative variation; this variation can clearly affect the pattern of the output spectrum by changing the location of the interference minima to either direction. In our experiment, the wavelength shift was around 16.44 nm toward the blue-shift, which agrees with the published work as in [24]. In the next examination steps, the length of NCF is increased by steps of 2 mm, the second sample NCF is 3.3 cm.

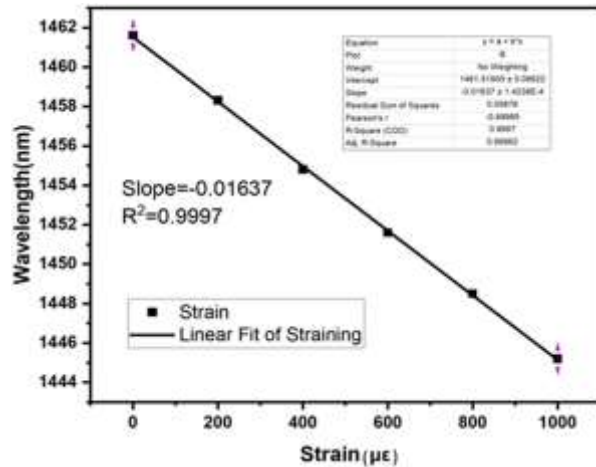


Figure (6): Linear fitting plot of the 3.1 cm NCF strain sensor

This sensor revealed an interference dip at 1455 nm, the extinction ratio of the 3.3 cm dip was 14.2 dB, strain the 3.3 cm sample in the range of 0-1000 με exhibited a total wavelength shift of 14.1 nm toward the shorter wavelengths direction, the shift of this sensor agreed with the 3.1 cm sample.

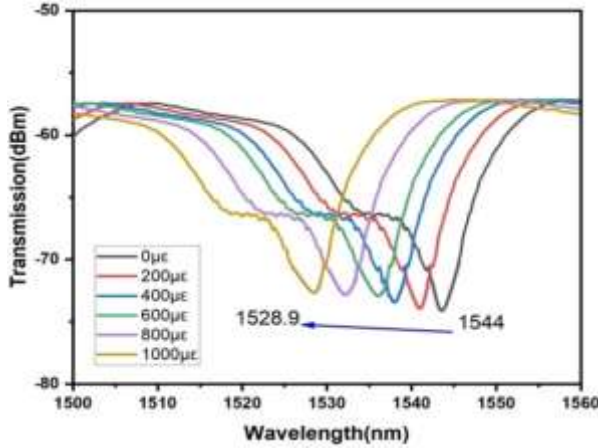


Figure (7): Spectral shift of the 3.3 cm NCF strain sensor.

The transmission spectrum of the 3.3 cm sensor length is illustrated in the figure (7), this sample revealed a wavelength sensitivity in response to strain of around  $-16.14 \text{ pm} / \mu\epsilon$ , employing the obtained results the linear fitting graph of the 3.3 cm NCF strain sensor is plotted, the 3.3 sensor showed an excellent linear behavior of spectral shift with strain as well, the linear regression coefficient of this sensor is  $R^2 = 0.9977$ , however the sensitivity is less than that of the 3.1 cm NCF strain sensor, the linear fitting graph of the 3.3 NCF strain sensor is depicted in figure (8).

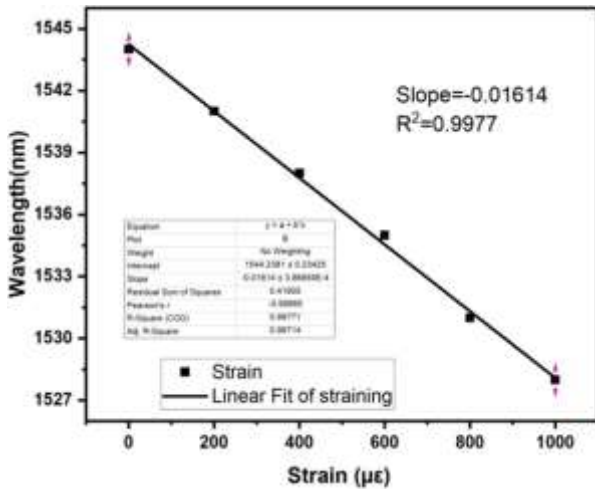


Figure (8): Linear fitting plot of the 3.3 cm NCF strain sensor

Proceeding to the next NCF sensing length examination, the NCF based strain sensor length is increased to 3.5 cm, repeating the next experimental procedure a piece of 3.5 cm NCF is fusion spliced between two standard SMF pigtail and strain in the same range of 0 - 1000  $\mu\epsilon$ .

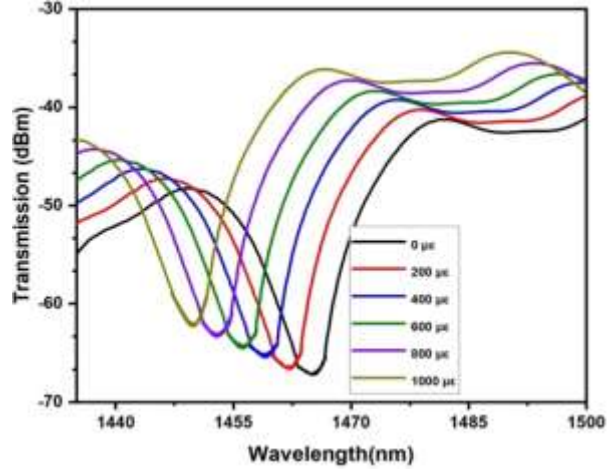


Figure (9): Spectral shift of the 3.5 cm NCF strain sensor

The 3.5 NCF strain sensor revealed an interference minima at 1465.4 nm, the extinction ratio of this sensor interference dip was 17.32 dB, by applying axial strain on the 3.5 cm sensor the total spectral shift was 15.4 nm toward blue-shift, the spectral shift of the 3.5 cm is expected to agree with the 3.3 cm sensing sample cm sample. The wavelength shift of the 3.5 cm sensor length is depicted in the figure (9).

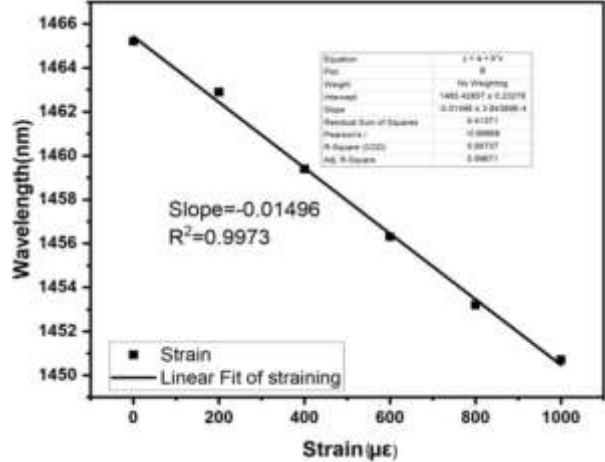


Figure (10): Linear fitting plot of the 3.5 cm NCF strain sensor

this sensor exhibited a spectral sensitivity in response to strain of around  $-14.96 \text{ pm} / \mu\epsilon$ , utilizing the attained results the linear fitting graph of the 3.5 cm NCF strain sensor is plotted, the 3.5 cm length strain sensor revealed a very good linearity with the spectral shift as a result of strain as well, the linear regression coefficient of this sensor is  $R^2 = 0.9973$ , noticing that the sensitivity is less than the sensitivity of the both

former samples, the 3.1 cm and the 3.3 cm, the linear fitting plot of the 3.5 cm NCF based strain sensor is depicted in figure (10).

By observing the behavior of the 3.1 cm, 3.3 cm and 3.5 cm NCF length based strain sensor, it's clearly obvious that the wavelength sensitivity in response to strain is decreasing as the length increases, this behavior can be expected as the length decreases, the applied strain can have greater impact on shorter segments [25]. To confirm this behavior, another sensing NCF sample length is examined which is the 3.7 cm sensor the transmission spectrum of the 3.7 cm sensing sample is depicted in figure (11). This sensing sample revealed an interference dip at 1541.5 nm, the extinction ratio of the dip was around 12.3 dB, by applying axial strain on this sensing sample in the selected range the interference dip suffered a blue-shift as well. The total wavelength shift of this sensor was around 11.9 nm, from the obtained result the linear fitting graph of the 3.7 cm NCF strain sensor is plotted, this sensor exhibited a very good linear behavior between the spectral shift and the strain the linear fitting graph of the 3.7 cm segment is shown in figure (12).

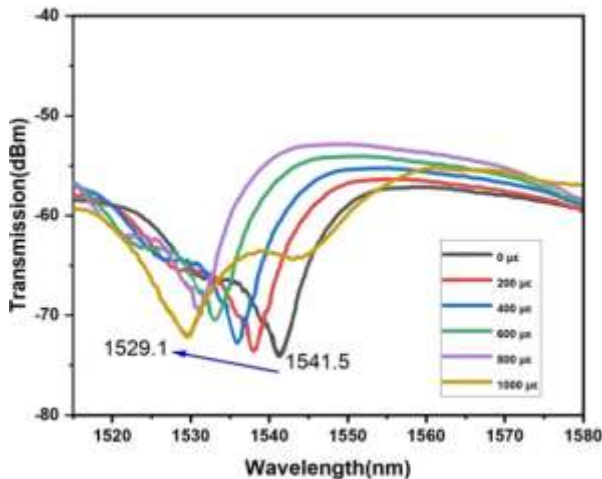


Figure (11): Spectral shift of the 3.7 cm NCF strain sensor

The determined sensitivity of the 3.7 cm NCF sample was  $-12.26 \text{ pm}/\mu\epsilon$ . From the all obtained results, it's obvious that the wavelength sensitivity is oppositely proportional to the sensing NCF length, this behavior confirms the importance of the sensing MMF length in opto-mechanical sensing application, selecting the best length can greatly affect the sensitivity of the proposed

sensor. It's necessary to mention that we have investigated the length influence by fixing the NCF diameter to  $125 \mu\text{m}$ .

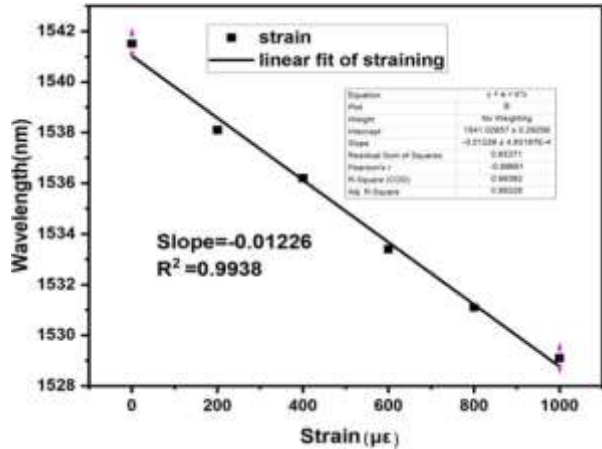


Figure (12): Linear fitting plot of the 3.7 cm NCF strain sensor

## 5. Conclusion

In conclusion, we have investigated the influence of the no-core fiber sensing length in strain sensors, a piece of no-core fiber fused between two single-mode fibers and axially strain, four different lengths were investigated by applying axial strain on each sample, the highest sensitivity obtained from the shortest NCF sensor length 3.1 cm which was  $-16.37 \text{ pm}/\mu\epsilon$ , this study is significant in designing NCF based strain sensors, to the best of our knowledge this is the first study of multimode NCF length influence on strain sensitivity.

**Conflict of interest** the authors declared no conflicts of interest

**Acknowledgement** this work is supported by university of Baghdad and the ministry of higher education and scientific researches of Iraq

## References

- [1] J. Li, W. Gan, H. Li, M. Xu, J. Liu, and A. Zhou, "Temperature compensated highly sensitive refractive index sensor based on Mach-Zehnder interferometer and FBG," *Optik*, vol. 241, p. 166838, Sep. 2021, doi: 10.1016/j.ijleo.2021.166838.
- [2] B. Du., "Highly sensitive hydrogen sensor based on an in-fiber Mach-Zehnder interferometer with polymer infiltration and Pt-

- loaded WO<sub>3</sub> coating,” *Opt. Express*, vol. 29, no. 3, p. 4147, Jan. 2021, doi: 10.1364/oe.417424.
- [3] B. Huang, Y. Wang, C. Liao, and Y. Wang, “Highly Sensitive Temperature Sensor Based on All-Fiber Polarization Interference Filter With Vernier Effect,” *IEEE Access*, vol. 8, pp. 207397–207403, 2020, doi: 10.1109/access.2020.3037522.
- [4] C. Zhou, Q. Zhou, B. Wang, J. Tian, and Y. Yao, “High-sensitivity relative humidity fiber-optic sensor based on an internal–external Fabry–Perot cavity Vernier effect,” *Opt. Express*, vol. 29, no. 8, p. 11854, Mar. 2021, doi: 10.1364/oe.421060.
- [5] A. Urrutia . “Novel Highly Sensitive Protein Sensors Based on Tapered Optical Fibres Modified with Au-Based Nanocoatings,” *Journal of Sensors*, vol. 2016, pp. 1–11, 2016, doi: 10.1155/2016/8129387.
- [6] Y. Tang et al., “High-sensitivity displacement sensing based on an OEO incorporating an unbalanced MZI,” *Optics & Laser Technology*, vol. 121, p. 105816, Jan. 2020, doi: 10.1016/j.optlastec.2019.105816.
- [7] Q. Wang and Y. Liu, “Review of optical fiber bending/curvature sensor,” *Measurement*, vol. 130, pp. 161–176, Dec. 2018, doi: 10.1016/j.measurement.2018.07.068.
- [8] M. Y. Rofianingrum, B. Widiyatmoko, E. Kurniawan, D. Bayuwati, and I. Afandi, “Fiber optic load sensor using microbend-deformer,” *J. Phys.: Conf. Ser.*, vol. 1191, p. 012007, Mar. 2019, doi: 10.1088/1742-6596/1191/1/012007.
- [9] M. R. A. Sanchez et al., “Fiber Bragg grating-based sensor for torque and angle measurement in a series elastic actuator’s spring,” *Appl. Opt.*, vol. 57, no. 27, p. 7883, Sep. 2018, doi: 10.1364/ao.57.007883.
- [10] H. Zhang, M. Zhang, J. Kang, X. Zhang, and J. Yang, “High Sensitivity Fiber-Optic Strain Sensor Based on Modified Microfiber-Assisted Open-Cavity Mach-Zehnder Interferometer,” *J. Lightwave Technol.*, pp. 1–1, 2021, doi: 10.1109/jlt.2021.3073412.
- [11] T. Liu, F. Pagliano, R. van Veldhoven, V. Pogoretskiy, Y. Jiao, and A. Fiore, “Integrated nano-optomechanical displacement sensor with ultrawide optical bandwidth,” *Nat Commun*, vol. 11, no. 1, May 2020, doi: 10.1038/s41467-020-16269-7.
- [12] Y. Guo, M. Chen, L. Xiong, X. Zhou, and C. Li, “Fiber Bragg grating based acceleration sensors: a review,” *SR*, vol. 41, no. 1, pp. 101–122, Feb. 2021, doi: 10.1108/sr-10-2020-0243.
- [13] C. Campanella, A. Cuccovillo, C. Campanella, A. Yurt, and V. Passaro, “Fibre Bragg Grating Based Strain Sensors: Review of Technology and Applications,” *Sensors*, vol. 18, no. 9, p. 3115, Sep. 2018, doi: 10.3390/s18093115.
- [14] Y. Zheng, X. Yang, W. Feng, and W. Fan, “Optical fiber refractive index sensor based on SMF-TCF-NCF-SMF interference structure,” *Optik*, vol. 226, p. 165900, Jan. 2021, doi: 10.1016/j.ijleo.2020.165900.
- [15] Y. Zhao, J. Zhao, and Q. Zhao, “High sensitivity seawater temperature sensor based on no-core optical fiber,” *Optical Fiber Technology*, vol. 54, p. 102115, Jan. 2020, doi: 10.1016/j.yofte.2019.102115.
- [16] Y. Zhao, J. Zhao, and Q. Zhao, “Review of no-core optical fiber sensor and applications,” *Sensors and Actuators A: Physical*, vol. 313, p. 112160, Oct. 2020, doi: 10.1016/j.sna.2020.112160.
- [17] F. Zhang et al., “A Refractive Index Sensitive Liquid Level Monitoring Sensor Based on Multimode Interference,” *Photonics*, vol. 7, no. 4, p. 89, Oct. 2020, doi: 10.3390/photonics7040089.
- [18] R. Bellini, C. V. S. Borges, B. Rente, and M. A. G. Martinez, “Optimized Multimode Interference Fiber Based Refractometer in A Reflective Interrogation Scheme,” *Proceedings*, vol. 2, no. 13, p. 1107, Dec. 2018, doi: 10.3390/proceedings2131107.
- [19] X. Dong, H. Du, X. Sun, Z. Luo, and J. Duan, “A Novel Strain Sensor with Large Measurement Range Based on All Fiber Mach-Zehnder Interferometer,” *Sensors*, vol. 18, no. 5, p. 1549, May 2018, doi: 10.3390/s18051549.
- [20] N. S. Fabian, A. B. Socorro-Leranz, I. D. Villar, S. Diaz, and I. R. Matias, “Multimode-Coreless-Multimode Fiber-Based Sensors: Theoretical and Experimental Study,” *J. Lightwave Technol.*, vol. 37, no. 15, pp. 3844–3850, Aug. 2019, doi: 10.1109/jlt.2019.2921609.
- [21] X. Dong, H. Du, X. Sun, and J. Duan, “Simultaneous Strain and Temperature Sensor

- Based on a Fiber Mach-Zehnder Interferometer Coated with Pt by Iron Sputtering Technology,” *Materials*, vol. 11, no. 9, p. 1535, Aug. 2018, doi: 10.3390/ma11091535.
- [22] L. Ma, Y. Qi, Z. Kang, and S. Jian, “All-Fiber Strain and Curvature Sensor Based on No-Core Fiber,” *IEEE Sensors J.*, vol. 14, no. 5, pp. 1514–1517, May 2014, doi: 10.1109/jsen.2014.2298553.
- [23] C. Campanella, A. Cuccovillo, C. Campanella, A. Yurt, and V. Passaro, “Fibre Bragg Grating Based Strain Sensors: Review of Technology and Applications,” *Sensors*, vol. 18, no. 9, p. 3115, Sep. 2018, doi: 10.3390/s18093115.
- [24] Y. Sun et al., “Dual-Parameters Optical Fiber Sensor With Enhanced Resolution Using Twisted MMF Based on SMS Structure,” *IEEE Sensors J.*, vol. 17, no. 10, pp. 3045–3051, May 2017, doi: 10.1109/jsen.2017.2673959.
- [25] K. Wang et al., “Advances in Optical Fiber Sensors Based on Multimode Interference (MMI): A Review,” *IEEE Sensors J.*, vol. 21, no. 1, pp. 132–142, Jan. 2021, doi: 10.1109/jsen.2020.3015086.

## دراسة تأثير طول الليف البصري منزوع القلب على الحساسية في متحسسات الاستطالة الضوئية

حسن مزاحم محمد      حنان جعفر طاهر

معهد الليزر للدراسات العليا / جامعة بغداد – بغداد / العراق

**الخلاصة:** تأثير الطول في الجزء المتحسس من الليف البصري منزوع القلب كمتحسس استطالة ضوئي تمت دراسته نظريا و عمليا وتم اخذ اربع عينات بأطوال مختلفة لليف البصري منزوع القلب بقطر 125 مايكرون و تم لحامها بين ليفين بصريين احادي الطول الموجي و تم تطبيق استطالة طولية على كل عينة و تبين من الدراسة ان العينة الاقصر و التي كان طولها 31 ملم هي الاكثر تحسسا للاستطالة الطولية على المحور اذ كانت الحساسية في تلك العينة 16.37 بيكومتر لكل وحدة استطالة. على حد علمنا هذه هي المرة الاولى التي يتم فيها دراسة تأثير الطول في متحسسات الاستطالة المبنية على الليف البصري منزوع القلب